Journal of
Materials Chemistry A

Accepted Manuscript

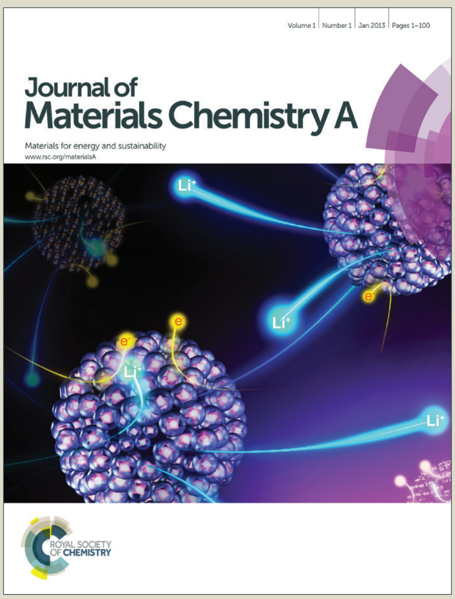

Journal of Materials Chemistry

Journal of Materials Chemistry A

Dynamic Article Links ►

Cite this: DOI: 10.1039/c0xx00000x

www.rsc.org/xxxxxx

ARTICLE TYPE

A Novel Strategy to Prepare Pt-SnO_2 Nanocomposite as Highly Efficient Counter Electrode for Dye-Sensitized Solar Cells

Xiao Chen[a†], Yu Hou[a†], Shuang Yang[a], Xiao Hua Yang*[a] and Hua Gui Yang*[a,b]

Received (in XXX, XXX) Xth XXXXXXXXX 20XX, Accepted Xth XXXXXXXXX 20XX

DOI: 10.1039/b000000x

A novel strategy was introduced to prepare Pt-SnO_2 nanocomposite, where the reduction of Pt^{4+} and the exfoliation of SnS_2 were finished in one step. The Pt-SnO_2 nanocomposite was applied as the counter electrode (CE) for dye-sensitized solar cells (DSCs). Compared with the energy conversion efficiency (E_{ff}) of SnO_2 CE based DSCs, the DSCs with Pt-SnO_2 CE showed an overall E_{ff} of 8.83%, giving an improvement of 198%. Meanwhile, better electrocatalytic activity towards I_3^-/I^- redox pairs than Pt CE indicated that the Pt-SnO_2 was a promising electrocatalyst for DSCs. Moreover, the low Pt content of Pt-SnO_2 composite would accelerate the large-scale applications of DSCs in the future.

1. Introduction

The dye-sensitized solar cells (DSCs) were firstly reported by O'Regan and Grätzel in 1991 and have achieved great advancement due to its low consumption, easy fabrication and powerful harvesting efficiency.[1, 2] To date, the highest energy conversion efficiency of DSCs is up to 13%.[3] Generally, there are three key components containing a sensitizer dye adsorbed nanocrystalline TiO_2 anode, an electrolyte containing iodide/triiodide (I^-/I_3^-) redox couple and a counter electrode (CE)[4, 5] in a typical DSC. As a superior CE material, platinum (Pt) is confirmed to own excellent catalytic activity for I_3^- reduction. However, the limited reserve and high cost of Pt severely restrict the large-scale application of the DSCs.[6] Therefore, many efforts have been devoted to exploring low-cost and high performance materials as replacements for Pt.

The CE materials investigated so far include different forms of carbon materials[7-9], conducting polymers[10], metal sulphides[11, 12], metal carbides[13], metal nitrides[14], metal phosphides[15] and metal oxides[16-20]. Compared to other materials, metal oxides have unique properties, such as high stability, low cost, environment-friendly and high catalytic activity.[21, 22] Among the common metal oxides, tin dioxide (SnO_2) as a wide bandgap semiconductor has been utilized as CE materials.[23, 24] Unfortunately, slightly low electrocatalytic activity of pure SnO_2 has restricted its application. Recently, Wu *et al*. prepared SnO_2 under N_2 atmosphere yielded energy conversion efficiency of 6.09%.[23] Pan et al. utilized a highly active nonstoichiometric $SnO_{2-\delta}$ as CE materials and achieved overall efficiency of 4.81%.[24] Meanwhile, loading traditional materials with Pt was also confirmed to be a useful method to improve the catalytic activity.[25] However, the Pt percentage is still too high to reach the target of low-cost.[26]

Here, we demonstrate a novel method to synthesize Pt-SnO_2 nanocomposite, and utilize it as CE materials in DSCs. In this method, the reduction of Pt^{4+} and the exfoliation of SnS_2 are finished in one step by the treatment of *n*-Butyllithium (*n*-BuLi) solution. The Pt-SnO_2 based solar cells yields an energy conversion efficiency of 8.83%, significantly higher than that of SnO_2 with an improvement of 198%. Moreover, the electrocatalytic activity of Pt-SnO_2 is even better than traditional Pt, indicating that the Pt-SnO_2 nanocomposite is a promising catalyst in DSCs. Meanwhile, indicatively coupled plasma atomic emission spectroscopy (ICP-AES) confirms that the weight ratio of Pt in Pt-SnO_2 composite is 23.1%, lower than previous reports (66.7%-93.0%).[26, 29]

2. Experimental

2.1 Preparation of Pt-SnO_2 nanocomposite

The Pt-SnO_2 nanocomposite was synthesized by a two-step method. Firstly, the mixture of 0.6 g SnS_2 nanoparticles (synthesized by a previous method[12]) and 140 mg $PtCl_4$ (Sinopharm, AR) were added into 50 mL hexane (Sinopharm, AR) in a argon atmosphere, followed by stirring for 3 h under 323 K. Secondly, 8 mL *n*-BuLi solution (1.6 M in hexane) was injected into the above solution under vigorous stirring for 24 h. After the reaction, black powder was obtained by filter, washed with hexane and ethanol and dried in air at 333 K. Finally, the product was sintered in a muffle furnace at 673 K for 30 min.

2.2 Preparation of counter electrodes

The Pt-SnO_2 coated counter electrodes were prepared on F-doped tin oxide conducting glass (FTO) substrate (NSG, 8 Ω/square) using a paste that made from the obtained Pt-SnO_2 power by screen-printing technology. The paste was made by mixing 0.5 g Pt-SnO_2 nanocomposites powder with 2.03 g anhydrous terpineol, 2.6 g ethyl celluloses in ethanol (10 wt%) and 8 mL ethanol followed by stirring, sonication and concentration. For comparison, the SnO_2 (AR) was purchased from Sinopharm and the SnO_2 CE films were prepared by the same procedure. The Pt electrode was prepared by drop-casting 0.5 mM H_2PtCl_6/ethanol solution on the clean FTO conductive glass. Subsequently, these formed films were annealed at 723 K for 30 min at ambient condition.

2.3 Fabrication of DSCs

The procedure of preparing the TiO_2 photoanode was described in detail as follow. Firstly, the FTO substrate was dipped into 40 mM $TiCl_4$ for 30 min at 343 K ($TiCl_4$ treatment). Then a 12 μm-thick layer of 20 nm-sized TiO_2 particles was loaded on the FTO by screen printer technique with an area of about 0.25 cm^2. After sintering at 398 K, the obtained layer was further coated with a 4 μm-thick scattering layer of 200 nm-sized TiO_2 particles (HEPTACHROMA, DHS-NanoT200) followed by sintering at 773 K. Another $TiCl_4$ treatment was carried followed by sintering at 773 K for 30 min. After cooling to 353 K, the photoanodes (TiO_2 films) were immersed in a 5×10^{-4} M solution of N719 dye (Solaronix SA, Switzerland) in acetonitrile/tert-butyl alcohol (V/V=1/1) for 24 h. DSCs were assembled together with the dye-sensitized TiO_2 electrode and the Pt-SnO_2 CE by a 25 μm-thick hot-melt film (Surlyn 1702, DuPont) and sealed up by heating. The cell internal space was filled with typical liquid electrolytes using a vacuum pump. The liquid electrolyte was composed of 0.60 M 1-butyl-3-methylimidazolium iodide, 0.03 M I_2, 0.50 M 4-tert-butyl pyridine, and 0.10 M guanidinium thiocyanate with acetonitrile as the solvent. The assembled DSCs were used for the photocurrent-voltage test with an active area of 0.25 cm^2. For electrochemical impedance spectroscopy (EIS) measurement, the symmetrical dummy cells were assembled by two identical CEs clipping the above liquid electrolyte.[25]

2.4 Characterization

The morphology and structure of the samples were characterized by high-resolution transmission electron microscopy (HRTEM, JEOL JEM-2010F, F20, 200 kV) and field emission scanning electron microscopy (FESEM, HITACHI S4800) and X-ray diffraction (XRD, Bruker D8 Advanced Diffractometer, Cu Kα radiation, 40 kV). The current-voltage tests of DSCs were performed under one sun condition using a solar light simulator (Oriel, 91160, AM 1.5 globe). The power of the simulated light was calibrated to 100 $mW\cdot cm^{-2}$ using a Newport Oriel PV reference cell system (model 91150 V). The EIS experiments were measured with dummy cells in the dark by using an electrochemical workstation (Parstat 2273, Princeton). The frequency range of EIS experiments was from 100 mHz to 1 MHz with an AC modulation signal of 10 mV and bias DC voltage of 0.60 V. The curves were fitted by the Zview software. Cyclic voltammetry (CV) was conducted in a three-electrode system in an acetonitrile solution of 0.1 M $LiClO_4$, 10 mM LiI, and 1 mM I_2 at a scan rate of 20 mV s^{-1} by using a BAS 100 B/W electrochemical analyzer. Platinum served as a CE and the Ag/Ag^+ couple was used as a reference electrode. Tafel polarization curves were measured with dummy cells in the dark using an electrochemical workstation (Parstat 2273, Princeton). Element analysis was conducted by indicatively coupled plasma atomic emission spectroscopy (ICP-AES, Vanan 710). The chemical states of elements in nanocomposites were analysed using X-ray photoelectron spectroscopy (XPS, Kratos Axis Ultra DLD), and the binding energy of the C 1s peak at 284.8 eV was taken as an internal reference. The nitrogen sorption isotherms were measured by a Micromeritics ASAP 2010N system.

3. Results and discussion

3.1. Preparation and characterization of Pt-SnO_2 nanocomposite

The schematic diagram of the synthesis of Pt-SnO_2 was shown in Fig. 1A. In this procedure, in order to bind the Pt precursors from the solution on the SnO_2 surface and obtain ultrafine dispersions of Pt nanocrystallites, SnS_2 nanosheets were utilized as raw materials because sulfur exhibited a strong affinity for noble metals owing to a soft acid-soft base interaction.[25, 27] The *n*-BuLi solution functioned not only as a strong reducing agent, providing a reduced condition to reduce the Pt^{4+} but also as an exfoliation agent. SnS_2 was one kind of layered transition metal dichalcogenides (LMDCs). The *n*-BuLi solution offered Li^+, which could intercalate inside the LMDCs and crush the bulk material into small particles.[28] Residual sulfur can be completely removed from the product by heat-treatment.

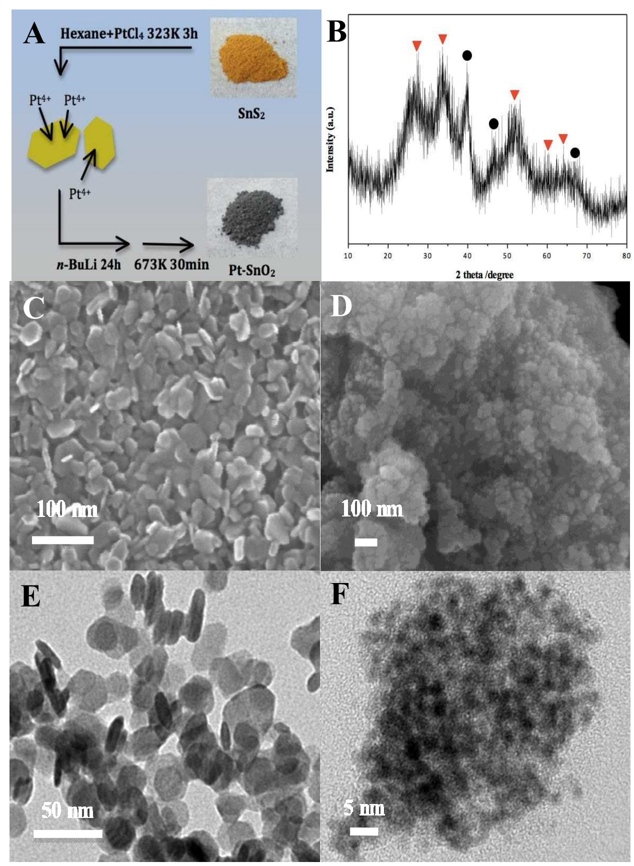

Fig. 1 (A) Schematic illustration of the Pt-SnO_2 synthesis procedure, **(B)** XRD patterns of the synthesized Pt-SnO_2 nanocomposite (red triangle: peaks of SnO_2, black circle: peaks of Pt), **(C,E)** SEM and TEM images of raw SnS_2 nanosheets, **(D,F)** SEM and TEM images of the synthesized Pt-SnO_2 nanocomposite.

The overall morphology of both SnS_2 nanosheets and Pt-SnO_2 nanocomposite were analyzed using the typical scanning electron microscope (SEM) and the transmission electron microscopy (TEM), shown in Fig. 1. The raw SnS_2 nanosheets present typically hexagonal structure and the mean diameter is in the range of 20-30 nm, which can be confirmed by the TEM image (see Fig. 1E). After the treatment of *n*-BuLi solution, the bulk materials were exfoliated and crushed into uniform ultra-small particles, whose average diameter was around 2-3 nm (see Fig. 1D and Fig. 1F). From the X-ray diffraction (XRD) pattern (see Fig. 1B) of the Pt-SnO_2 nanocomposite, it can be seen that all diffraction peaks of the typical XRD pattern could be attributed to SnO_2 (JCPDS No. 41-1445) and Pt (JCPDS No. 65-2868), respectively. The ICP-AES measurement indicates that the weight ratio of Pt in Pt-SnO_2 nanocomposite is 23.1%.

In order to investigate the impact of sintering (723K) in preparation of CEs, the obtained Pt-SnO_2 nanocomposite was further calcined at 723K for 30min. SEM images and XRD pattern indicate that no obvious changing in morphology and composition (see Fig. S1). The valence state of the Pt after the second thermal treatment is Pt^0 and Pt (Ⅳ), analyzed by XPS (Fig. S2). The nitrogen sorption isotherms indicate the specific surface area of Pt-SnO_2 is 36.96 m^2/g, much larger than that of Pt (10.48 m^2/g) in previous report.[18] Furthermore, SEM images of Pt-SnO_2 and Pt CEs on FTO are shown in Fig. S1. Both Pt-SnO_2 nanocomposites and Pt nanoparticles disperse well on the surface of FTO. In order to compare the surface area of Pt-SnO_2 and Pt CEs, the mass of materials on different CEs are obtained by ICP-AES measurement. As a result, the surface area of Pt-SnO_2 CE (1.63 cm^2) is larger than that of Pt CE (0.63 cm^2), and the detail data are summarized in Table. S1.

3.2 Photovoltaic measurement

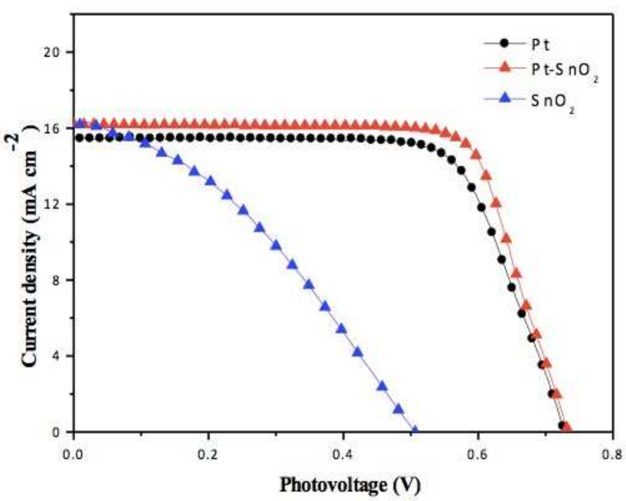

Fig. 2 *J–V* characteristics of the DSCs with Pt CE, Pt-SnO_2 CE and SnO_2 CE, measured at 100 mW cm^{-2}.

The photocurrent-voltage (J-V) curves (Fig. 2) of the DSCs with different CEs were measured under illumination at 100 mW cm^{-2} and the detailed photovoltaic parameters were summarized in Table 1. As shown in Fig. 2, the DSC using SnO_2 CE shows an overall energy conversion efficiency (E_{ff}) of 2.96%, which indicates that the pure SnO_2 CE present poor electrocatalytic activity for I_3^- reduction. In contrast, the short-circuit photocurrent density (J_{sc}), open-circuit voltage (V_{oc}), fill factor (FF) and E_{ff} of DSCs based on Pt-SnO_2 CEs are 16.24 mA cm^{-2}, 731 mV, 0.74 and 8.83%, respectively. The higher V_{oc} and FF of Pt-SnO_2 may be due to the more interfacial active sites of Pt-SnO_2 CEs. It is worth noting that the E_{ff} of Pt-SnO_2 CEs is even larger than that of Pt CEs based DSCs (8.04%), indicating that the Pt-SnO_2 CEs exhibit better electrocatalytic activity than that of Pt CEs.

Table 1 Photovoltaic parameters of DSCs with different counter electrodes, measured at 100 mW cm^{-2} illumination.

CE	J_{SC} mA/cm^2	V_{OC} mV	*FF*	*η* %	R_s Ω	R_{ct} Ω	*C* μF
SnO_2	16.18	506	0.36	2.96			
Pt	15.50	725	0.71	8.04	21.95	3.70	21.87
Pt/SnO_2	16.24	731	0.74	8.83	21.46	3.59	38.00

3.3 Electrochemical measurements

In order to further investigate the different catalytic activity for triiodide reduction between the Pt-SnO_2 CEs and Pt CEs, EIS technique was employed and the Nyquist plots of the symmetrical cells are shown in Fig. 3. After fitting the spectra with an EIS spectrum analyzer, the values of the series resistance (R_s), the charge-transfer resistance (R_{ct}) and constant phase element (CPE) are obtained and summarized in Table 1. The equivalent circuit used to fit the experimental EIS data is shown in the inset of Fig. 3. R_s is mainly composed of the bulk resistance of CEs materials, resistance of FTO glass substrate and contact resistance, etc. The R_s of Pt-SnO_2 CEs is 21.46 Ω, while this value of Pt CEs is 21.95 Ω. Smaller R_s indicates that Pt-SnO_2 CEs have a faster electron transfer kinetics and better electrical conductivity than Pt CEs, which is consistent with the improvement of J_{sc}.[16] R_{ct} is a measure of the ease of electron exchange between the counter electrode and the electrolyte and thus varies inversely with the triiodide reduction activity of the CEs. The slightly lower R_{ct} of Pt-SnO_2 CEs leads to a better catalytic activity, explaining the better performance than that of Pt CEs based cells.[17] Although the difference of R_s and R_{ct} between Pt-SnO_2 and Pt CEs isn't obvious, the larger capacitance (C) of Pt-SnO_2 CE indicates a higher surface area than that of Pt CE, which is responsible for higher E_{ff}, in agreement with the measured surface area of various CEs in Table S1.[30] In conclusion, low R_s, low R_{ct} and high C resulted in the high power-conversion efficiency of DSCs with Pt-SnO_2 CE and agreed well with the photovoltaic experiments.

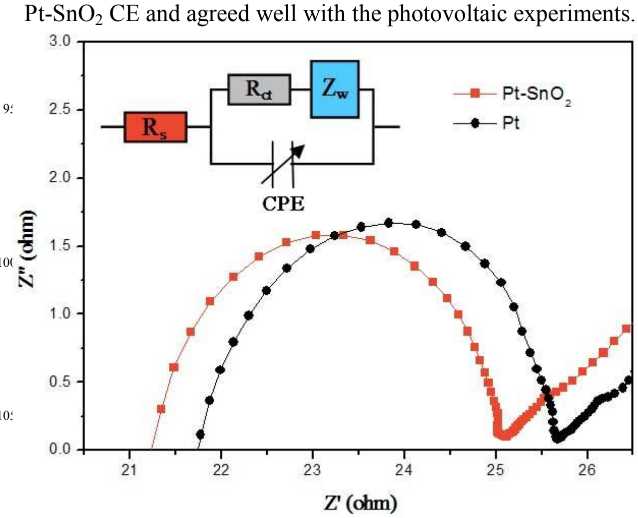

at

100 mW cm^{-2} light intensity.

As a powerful electrochemical characterization method, Tafel polarization measurement was carried out to further examine the interfacial charge-transfer properties of the triiodide/iodide couple on the electrode surface with dummy cells fabricated with two identical electrodes (CE//electrolyte//CE). The Tafel curves in Fig. 4 show that the current density (J) is a logarithmic function of the voltage (U). Generally, the Tafel curve is composed of three zones via the value of overpotential: the polarization zone at low overpotential, Tafel zone at middle overpotential (with a sharp slope), diffusion zone at high overpotential. In Tafel zone, the curve of the Pt-SnO_2 CE shows a larger slope than the conventional Pt CE, indicating the presence of a large exchange current density on the electrode surfaces, which means that Pt-SnO_2 CE has a higher catalytic activity than the Pt CE. Moreover, the current densities of Pt-SnO_2 CE obtained in all three zones are higher, which is consistent with the results of photovoltaic and EIS measurements.[25]

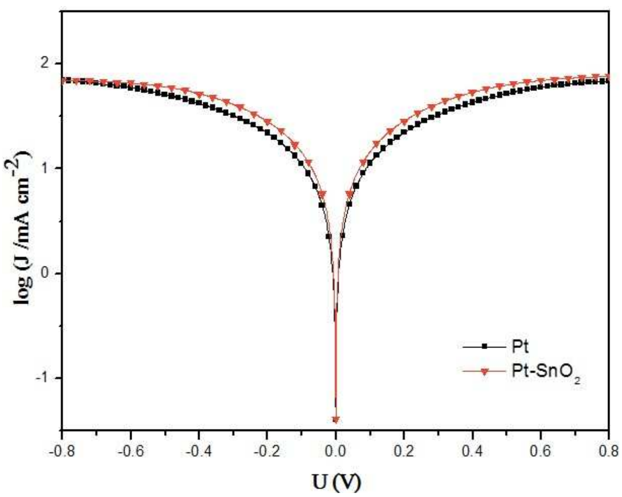

Fig. 4 Tafel curves of the symmetrical cells fabricated with two identical counter electrodes of Pt-SnO_2 and Pt nanoparticles, respectively.

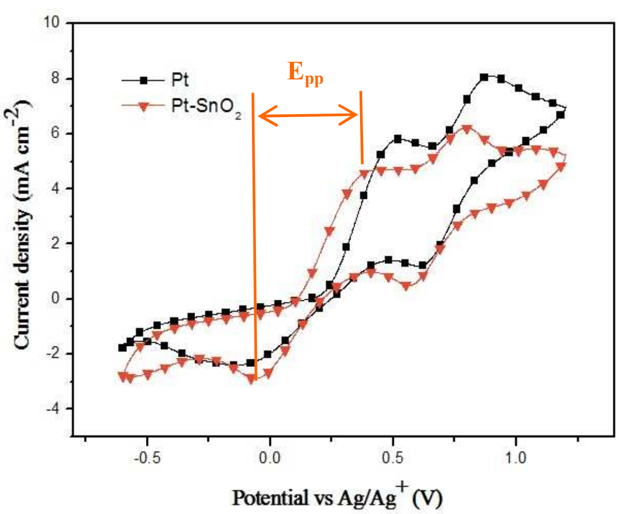

Fig. 5 Cyclic voltammograms of iodide species for Pt-SnO_2 and Pt electrodes.

The cyclic voltammetry (CV) measurement was further carried out in a three-electrode system to evaluate the electrocatalytic properties of the Pt-SnO_2 CE (Fig. 5). Typical curves with two pairs of oxidation and reduction peaks are obtained for Pt-SnO_2 CE. The left peak is corresponding to the redox reaction of eqn (1), while the right one is corresponding to the reaction of eqn (2).

$$I_3^- + 2e = 3I^- \quad (1)$$

$$3I_2 + 2e = 2I_3^- \quad (2)$$

The peak-to-peak splitting (E_{pp}) of Pt-SnO_2 CE is 492 mV, much smaller than that of bare Pt CE (670 mV), suggesting that the electrocatalytic activity and reversibility of I_3^-/I^- redox reaction on Pt-SnO_2 CE are better.[12]

Conclusions

In summary, we have demonstrated a novel method to synthesize Pt-SnO_2 nanoparticles, where the reduction of Pt^{4+} and the exfoliation of SnS_2 are performed in one step (the treatment of *n*-BuLi). As a high-efficient CE material for DSCs, Pt-SnO_2 composite exhibit better photovoltaic performance than the conventional Pt electrode. Furthermore, the low Pt content of Pt-SnO_2 composite is correspond to the objective of low-cost and this design strategy would be very promising to pave the way to the large-scale commercialization of DSCs.

Acknowledgement

This work was financially supported by National Natural Science Foundation of China (21373083, 21203061), SRF for ROCS, SEM, SRFDP, Programme for Professor of Special Appointment (Eastern Scholar) at Shanghai Institutions of Higher Learning, Fundamental Research Funds for the Central Universities (WD1313009, WD1214036), and China Postdoctoral Science Foundation (2013T60425).

Notes and references

[a] *Key Laboratory for Ultrafine Materials of Ministry of Education, School of Materials Science and Engineering, East China University of Science and Technology, 130 Meilong Road, Shanghai, 200237 (China). Fax: (+86)21-6425-2127; Tel: (+86)21-6425-2127; E-mail: hgyang@ecust.edu.cn*

[b] *Centre for Clean Environment and Energy, Gold Coast Campus, Griffith University, Queensland 4222 (Australia)*

† These authors contributed equally to this work.

1. B. O'Regan and M. Grätzel, *Nature*, 1991, **353**, 737-740.
2. M. Grätzel, *Nature*, 2001, **414**, 338-344.
3. S. Mathew, A. Yella, P. Gao, R. Humphry-Baker, B. F. E. Curchod, N. Ashari-Astani, I. Tavernelli, U. Rothlisberger, Md. K. Nazeeruddin and M. Grätzel, *Nature chemistry*, 2014, **6**, 242-247.
4. G. R. Li, F. Wang, Q. W. Jiang, X. P. Gao and P. W. Shen, *Angew. Chem. Int. Ed.*, 2010, **49**, 3653-3656.
5. H. Zhang, Y. Wang, D. Yang, Y. Li, H. Liu, P. Liu, B. J. Wood and H. Zhao, *Adv. Mater.*, 2012, **24**, 1598-1603.
6. K. C. Huang, Y. C. Wang, R. X. Dong, W. C. Tsai, K. W. Tsai, C. C. Wang, Y. H. Chen, R. Vittal, J. J. Lin and K. C. Ho, *J. Mater. Chem.*, 2010, **20**, 4067-4073.
7. P. Joshi, Y. Xie, M. Ropp, D. Galipeau, S. Bailey and Q. Q. Qiao, *Energy Environ. Sci.*, 2009, **2**, 426-429.

8. M. Wu, X. Lin, T. Wang, J. Qiu and T. Ma, *Energy Environ. Sci*., 2011, **4**, 2308-2315.
9. L. Kavan, J. H. Yum and M. Grätzel, *ACS Nano*, 2011, **5**, 165-172.
10. S. Ahmad, J. H. Yum, H. J. Butt, M. K. Nazeeruddin and M. Grätzel, *ChemPhysChem*, 2010, **11**, 2814-2819.
11. M. Wang, A. M. Anghel, B. T. Marsan, N. L. Cevey Ha, N. Pootrakulchote, S. M. Zakeeruddin and M. Grätzel, *J. Am. Chem. Soc*., 2009, **131**, 15976-15977.
12. X. Chen, Y. Hou, B. Zhang, X. H. Yang and H. G. Yang, *Chem. Commun.*, 2013, **49**, 5793-5795.
13. M. Wu, X. Lin, A. Hagfeldt and T. Ma, *Angew. Chem. Int. Ed.*, 2011, **50**, 3520-3524.
14. A. M. Hung, N. A. Konopliv and J. N. Cha, *Langmuir*, 2011, **27**, 12322-12328.
15. M. Wu, J. Bai, Y. Wang, A. Wang, X. Lin, L. Wang, Y. Shen, Z. Wang, A. Hagfeldt and T. Ma, *J. Mater. Chem*., 2012, **22**, 11121-11127.
16. Y. Hou, Z. P. Chen, D. Wang, B. Zhang, S. Yang, H. F. Wang, P. Hu, H. J. Zhao and H. G. Yang, *Small*, 2014, **10**, 484-492.
17. Y. Hou, D. Wang, X. H. Yang, W. Q. Fang, B. Zhang, H. F. Wang, P. Hu, H. J. Zhao and H. G. Yang, *Nat. Commun*., 2014, **4**, 1583.
18. B. Zhang, D. Wang, Y. Hou, S. Yang, X. H. Yang, J. H. Zhong, J. Liu, H. F. Wang, P. Hu, H. J. Zhao and H. G. Yang, *Sci. Rep.*, 2013, **3**, 1836.
19. M. Wu, X. Lin, A. Hagfeldt and T. Ma, *Chem. Commun.*, 2011, **47**, 4535- 4537.
20. L. Cheng, Y. Hou, B. Zhang, S. Yang, J. W. Guo, L. Wu and H. G. Yang, *Chem. Commun.*, 2013, **49**, 5945-5947.
21. X. Lin, M. Wu, Y. Wang, A. Hagfeldt and T. Ma, *Chem. Commun.*, 2011, **47**, 11489-11491.
22. S. Yun, H. Zhang, H. Pu, J. Chen, A. Hagfeldt and T. Ma, *Adv. Energy Mater.*, 2013, **3**, 1407-1412.
23. M. Wu, X. Lin, W. Guo, Y. Wang, L. Chu, T. Ma and K. Wu, *Chem. Commun.*, 2013, **49**, 1058-1060.
24. J. Pan, L. Z. Wang, C. Y. Jimmy, G. Liu, and H. M. Cheng, *Chem. Commun.*, 2014, **50**, 7020-7023.
25. J. W. Guo, B. Zhang, Y. Hou, S. Yang, X. H. Yang and H. G. Yang, *J. Mater. Chem. A*, 2013, **1**, 1982–1986.
26. L. -Y. Chang, C. -P. Lee, K. -C. Huang, Y. -C. Wang, M. -H. Yeh, J. -J. Lin and K. -C. Ho, *J. Mater. Chem.*, 2012, **22**, 3185-3191.
27. J. T. Miller and D. C. Koningsberger, *J. Catal.*, 1996, **162**, 209-219.
28. G. Eda, H. Yamaguchi, D. Voiry, T. Fujita, M. Chen and M. Chhowalla, *Nano letters*, 2011, **11**, 5111-5116.
29. K. -C. Huang, Y. -C. Wang, R. –X. Dong, W. –C. Tsai, K. –W. Tsai, C. –C. Wang, Y. –H. Chen, R. Vittal, J. –J. Lin and K. -C. Ho, *J. Mater. Chem.*, 2010, **20**, 4067-4073.
30. T. N. Murakami, S. Ito, Q. Wang, M. K. Nazeeruddin, T. Bessho, I. Cesar, P. Liska, R. Humphry-Baker, P. Comte, P. Pechy and M. Grätzel, *J. Electrochem. Soc.*, 2006, **153**, A2255-A2261.

TOC figure:

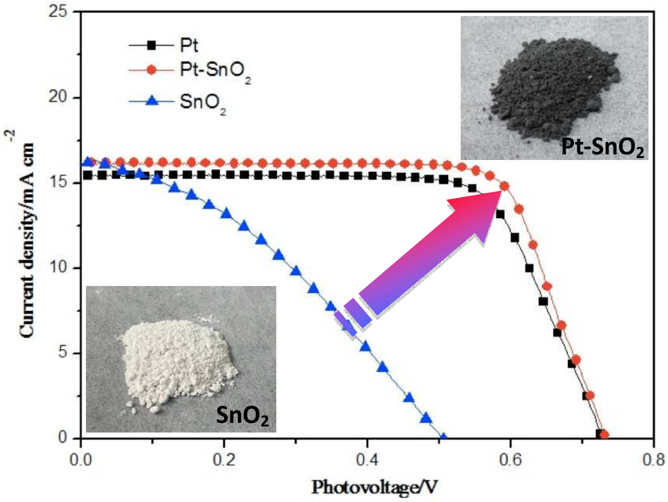

A novel strategy was introduced to prepare Pt-SnO_2 nanocomposite by combining reduction of Pt^{4+} and exfoliation of SnS_2 in one step. When the Pt-SnO_2 nanocomposite was applied as counter electrode (CE) for dye-sensitized solar cells (DSCs), energy conversion efficiency (E_{ff}) of 8.83% was achieved with an improvement of 198% by comparing with the E_{ff} of SnO_2 CE based DSCs. Meanwhile, better electrocatalytic activity towards I_3^-/I^- redox pairs than Pt CE indicated that the Pt-SnO_2 was a promising catalyst for DSCs. Moreover, the low Pt content of Pt-SnO_2 composite would accelerate the large-scale applications of DSCs in the future.